Diminishing returns epistasis among beneficial mutations decelerates adaptation

Hsin-Hung Chou,[1,*] Hsuan-Chao Chiu,[3] Nigel F. Delaney,[1] Daniel Segrè,[3,4] Christopher J. Marx[1,2†]

Supplemental Online Material

Materials and Methods
Plasmid and Strain Construction

All strains and plasmids used are indicated in Tables S1 and S2. All plasmids were constructed and maintained in *Escherichia coli* DH5α or 10-beta strains from New England Biolabs (Ipswich, MA, USA), and were transferred to (or from) *Methylobacterium extorquens* AM1 strains via conjugation using tri-parental matings with the helper strain pRK2073 (*21*).

Two engineered *Methylobacterium* (EM) strains, one pink and one white (defective carotenoid biosynthesis due to a disrupted $crtI^{502}$ allele generated by *cre*-mediated excision of the majority of IS*phoA/hah*-Tc from the original white S234-13 transposon mutant) (*22*), were used as ancestors in order to have a neutral marker as a lineage label to detect possible contamination across populations. A pink strain of WT (*i.e.*, CM501) (*23*) deleted for the *mptG* gene (encoding β-ribofuranosylaminobenzene 5′-phosphate synthase) (*24*) required for biosynthesis of the tetrahydromethanopterin cofactor used by the original formaldehyde oxidation pathway, CM508, was generated previously (*23*). The Δ*mptG* allele was introduced into the white WT strain, CM502 (*23*), using a previously described *cre-lox* allelic exchange vector pCM253 (*14*) carrying a Δ*mptG::kan* allele, and then removing the *kan* cassette using the pCM157 *cre*-expression vector (*25*) to ultimately generate the white, unmarked Δ*mptG* strain CM624. The original plasmid (pCM106) generated to express the GSH pathway from the strong, native promoter for methanol dehydrogenase (*i.e.*, P_{mxaF}) carried the *tetAR* tetracycline resistance marker, which alone causes poor growth (*14*). Therefore a new plasmid, pCM410 (fig. S6), was generated by replacing *tetAR* with the kanamycin resistance marker (*kan*) from pCM160 (*26*). This plasmid was introduced into CM508 and CM624, respectively, to generate the two EM strains used as ancestors for these populations, CM701 and CM702.

To facilitate fluorescence-based fitness assays using flow cytometry (*27*), fluorescent EM strains isogenic to CM701 and CM702 except for bearing the *mCherry* gene expressed from the moderate strength, constitutive P_{tacA} promoter in the *katA* locus were generated as above except for starting with two *mCherry*-marked WT strains: CM1175 (pink-colored) and CM1176 (white-colored) (*27*). Deletion of the *mptG* gene from these strains (using pCM253 and pCM157) resulted in CM1225 and CM1226, respectively. The pCM410 plasmid was then conjugated into these Δ*mptG* strains to generate fluorescent EM strains CM1231 and CM1232. The *mCherry* fluorescent marker was selectively neutral under tested conditions.

To facilitate genetic manipulations with CM1145, a plasmid-free strain derived from this evolved isolate was obtained by propagating CM1145 in succinate liquid media without either kanamycin or methanol. In the absence of either selection to maintain pCM410, cells grown in liquid media for 18 generations were first plated on agar plates supplemented with succinate. Isolates were then tested for their ability to grow on methanol agar plates or succinate plates supplemented with kanamycin (50 μg/ml). One such isolate, CM1276, unable to grow on either condition was chosen. This plasmid-free strain did not appear to acquire additional fitness-affecting mutations as reintroducing pCM410 bearing the $fghA^{EVO}$ evolved allele into CM1276 resulting in a strain as fit as the original CM1145. The two plasmid-free strains, CM624 (by definition $pntAB^{WT}$, gsh^{WT}, GB^{WT}) and CM1276 ($pntAB^{EVO}$, $gshA^{EVO}$, GB^{EVO}) served as the two starting points to construct, in a stepwise fashion, the 14 strains with one, two, or three evolved alleles. Allelic exchange plasmids containing the ancestral allele of *pntAB* or *gshA* in

pCM433 (*23*) were made as follows. The 607-bp fragment containing *pntA^{WT}* from CM501 was PCR amplified by primers HCAMp29 (5′-TCTCGAGTTCTGGATCTTGCCCAGTTC-3′) and HCAMp30 (5′-TGAGCTCCCACGAGCAGACCTATC-3′). The resulting PCR product was digested by *Xho*I and *Sac*I, and then ligated into the *Xho*I-*Sac*I digested pCM433 backbone to generate pHC35. The 584-bp fragments containing *gsh^{WT}* from CM501 was PCR amplified by primers pHCAMp31 (5′-CGAGCTCGCCCTCATATGGAAC-3′) and pHCAMp32 (5′-ACTCGAGATCGTCTCCACCCTGATC-3′). The resulting PCR product was digested by *Sac*I and *Xho*I, and then ligated into the *Sac*I-*Xho*I digested pCM433 backbone to generate pHC37. Constructs to introduce *pntAB^{EVO}* and *gshA^{EVO}* were generated in the same manner previously (*i.e.*, pHC36 and pHC38) (*15*). Subsequent to generating the desired chromosomal genotype, strains bearing either *fghA^{WT}* or *fghA^{EVO}* could be generated by simply reintroducing either the original pCM410 plasmid or the evolved pCM410.1145 plasmid that had been conjugated into *E. coli* from CM1145. All intermediate and final strains from this process and the order of introductions to generate the full set of allele combinations are indicated below in Table S1.

Media for Growth Experiments

One liter of growth media consisted of 1 ml of the trace metal solution, 100 ml of phosphate buffer (25.3 g of K_2HPO_4 and 22.5 g of NaH_2PO_4 in 1 liter of deionized water), 100 ml of sulfate solution (5 g of $(NH_4)_2SO_4$ and 0.98 g of $MgSO_4$ in 1 liter of deionized water), 799 ml of deionized water, and the desired carbon source (*27*). The trace metal solution used during the evolution experiments (per 100 ml, maintained at pH 5 after each addition) consisted of 12.738 g of EDTA disodium salt dihydrate, 4.4 g of $ZnSO_4 \cdot 7H_2O$, 1.466 g of $CaCl_2 \cdot 2H_2O$, 1.012 g of $MnCl_2 \cdot 4H_2O$, 0.22 g of $(NH_4)_6Mo_7O_{24} \cdot 4H_2O$, 0.314 g of $CuSO_4 \cdot 5H_2O$, 0.322 g of $CoCl_2 \cdot 6H_2O$, and 0.998 g of $FeSO_4 \cdot 7H_2O$ in 1 liter of deionized water (*27*). Effective concentrations of trace metals in this solution, however, were subsequently shown to be unstable due to the light-dependent degradation of the metal chelator EDTA (*15*). To ensure the consistency of testing conditions, a robust formulation with slight modifications was hence developed (*15*) and applied for all phenotypic assays described here. This modified trace metal mix (per 100 ml) consisted of 10 ml of 179.5 mM $FeSO_4$ (5x relative to above recipe), 80 ml of premixed metal mix (12.738 g of EDTA disodium salt dihydrate, 4.4 g of $ZnSO_4 \cdot 7H_2O$, 1.466 g of $CaCl_2 \cdot 2H_2O$, 1.012 g of $MnCl_2 \cdot 4H_2O$, 0.22 g of $(NH_4)_6Mo_7O_{24} \cdot 4H_2O$, 0.314 g of $CuSO_4 \cdot 5H_2O$, and 0.322 g of $CoCl_2 \cdot 6H_2O$ in 1 liter of deionized water, pH 5), and 10 ml of deionized water.

Experimental Evolution Regime

The evolution experiment consisted of eight replicate populations, designed as F1 through F8. The odd and even-numbered populations were founded by the pink-colored and white-colored EM strains CM701 and CM702, respectively. The alternation of the color marker was designed to aid in detecting contamination or mislabeling flasks. All populations were grown on 15 mM methanol in 9.6 ml of growth media contained in 50 ml Erlenmeyer flasks and incubated in a 30 °C shaking incubator at 225 rpm. An inoculum of 1/64 the total volume (150 µl) was transferred into 9.45 ml fresh medium, thereby permitting an average of six generations during each growth cycle. Due to the slow growth of the EM strains, during the first 300 generations of evolution these transfers occurred every four days. Once all populations could sustain a two day cycle (generation 300), the transfer cycle was switched to every two days thereafter to maintain selection primarily upon exponential phase. Populations were sampled periodically and preserved with 8% DMSO at –80 °C for later analysis. Three random isolates were obtained from each population at generations 60, 120, 300, and 600 to estimate the adaptive trajectories of populations (Table S2). Among the three random isolates, one was chosen randomly to characterize changes in growth rate, yield, and cell size.

Fitness Assays

Prior to competition experiments, all strains were acclimated in growth medium supplemented with carbon sources used in the ensuing assays. Competition experiments were performed by following a previously described procedure (*27*) with the following adjustment due to the slow growth of the EM

strain on methanol. The duration for competition experiments in growth media supplemented with methanol and succinate was four days and two days, respectively. After one round of acclimation, test strains and a fluorescent reference strain were mixed by a 1:1 volume ratio, diluted 1:64 into 9.6 ml of fresh media which were incubated under the conditions described above. The frequencies of nonfluorescent cells in mixed populations were measured by passing population samples before (F_0) and after (F_1) competition growth through a BD LSR II flow cytometer (BD Biosciences, San Jose, CA, USA) for at least $5 \cdot 10^4$ cell counts per sample. Fitness values (W) relative to the reference strain were calculated by a previously described equation assuming an average of 64-fold size expansion of mixed populations during competitive growth (*27*):

$$W = \log\left(\frac{F_1 \cdot 64}{F_0}\right) \Big/ \log\left(\frac{(1 - F_1) \cdot 64}{1 - F_0}\right)$$

Because the color marker was selectively neutral across genetic backgrounds, phenotypes of the WT strain and the EM strain were assayed based on their white-colored isogenic variants. The white-colored fluorescent EM strains CM1232 was used regularly as the reference strain to measure fitness of evolved isolates from the F populations, the 16 mutational combination strains, and the WT strain. To measure fitness of the EM strain, evolved isolates from F populations, and the WT strain during growth on succinate, growth media for the acclimation phase were supplemented with 3.5 mM disodium succinate plus kanamycin (25 μg/ml) to prevent spontaneous loss of pCM410 in the absence of selection.

Competition experiments then proceeded in growth media supplemented with just 3.5 mM disodium succinate. Because the WT strain was sensitive to kanamycin, the white isogenic variant, CM611 (*27*), bearing the *katA::kan* marker was used instead, as it has been shown that this strain is neutral in the WT genetic background during growth on either methanol or succinate (*27*).

Selection of CM1145 as the EVO strain for further analysis

Based upon fitness assays for three isolates from each population at generation 600, we selected one of the fittest of these (CM1145) to pursue further here, as well as in earlier work (*15*). Other strains isolated subsequently from the F4 population at 600 generations (CM1735, CM1736, CM1737) were not statistically distinguishable from CM1145 in terms of fitness (Table S2).

Enzyme Assays

The activities of FlhA (*28*) and FghA (*29*) were assayed as described from three biological replicates using cells harvested from mid-exponential phase cultures. Cells were collected through centrifugation at $10,000 \times$ g for 10 min, frozen at -80 °C, and used for enzyme assays within a week. Before physical disruption, cell material was suspended in 50 mM Tris-HCl buffer (pH 7.5). Cell extracts were prepared using a French pressure cell at 10^8 Pa (two times, 4 °C) and then centrifuged at $13,000 \times$ g, 4 °C for 15 min to remove cell debris. The total protein concentration in the extracts was assayed using the Bradford method (*30*). Kinetic analyses of FlhA and FghA activities over 10 min at 30 °C were monitored in 200 μl reaction mixtures using a SpectraMax M5 Plate Reader (Molecular Devices, Sunnyvale, CA, USA).

Determination of Cell Length and Morphology

Cells from mid-exponential phase cultures were collected by centrifugation at $10,000 \times$ g for 10 min, suspended in 50 mM Tris-HCl buffer (pH 7.5) plus 8% DMSO (v/v) as cryo-protectant, and then frozen at -80 °C until further use. Analysis of cells morphology on a LSR II flow cytometer (BD Biosciences) was performed following a previously described method (*31*). Before analysis, Fluoresbrite® YO Carboxylate Microspheres (Polysciences, Warrington, PA, USA) of 0.75, 1, 3, and 6 μm diameter were used to calibrate the instrument. The 1 μm fluorescent beads were added into all samples which served as the standard for data normalization. Forward scatter (FSC) measures were collected at low flow rates with an average of 250 events per second throughout data collection. Data were collected from least 8000 cells per sample and analyzed using FSCDiva Software 6.0 (BD

Biosciences). Relative measures of cell sizes were calculated by dividing the FSC geometric means of cells by those of the 1 μm fluorescent bead (*32*). For microscopy, cells were suspended in 50 mM Tris-HCl buffer (pH 7.5) and mounted on slides coated with either poly-lysine or 1% agarose. Microscopy was performed on a Zeiss Axioskope 40 microscope equipped with an AxioCam MRm camera (Carl Zeiss, Thornwood, NY, USA). Images were processed with the AxioVision 4.5 software (Carl Zeiss). For each sample, the cell morphology of 560 cells was scored using ImageJ (*33*). The cell length was measured by the longitudinal axis across the cell body. A cell was considered as elongated when its cell length exceeds 6 μm (twice the normal cell length). A cell was defined as curved when the included angle of the longitudinal axis was less than 135°. A cell was scored as branched when protrusions occurred outside two cell poles. For branched cells, their cell length was measured by the longitudinal axis of the mother cell.

Strain Sequencing and Mutation Detection

Genomic DNA from strain CM1145 as well as the ancestral strain CM501 was sequenced via the Genome Analyzer (Illumina, San Diego, CA, USA) sequencing platform to generate 36 bp single end reads. For strain CM1145, a total of 21,893,037 reads were generated, which after quality filtering (*i.e.*, does or does not align) gave approximately ~68X coverage of the chromosome (coverage levels of the plasmids were equivalent to this after accounting for the fact that some are carried in multiple copies by the cell or suffered large deletions, thus skewing average coverage statistics). A description of the most profitable methods used to find mutations is given below, however, other methods (*e.g.*, other SNP calling software) and parameter settings were used but are not reported here as they either failed to identify as many mutations or merely performed as well.

SNP Detection

In order to detect single nucleotide changes in CM1145, the Illumina reads were aligned to the reference *M. extorquens* AM1 genome (Accession: CP001510.1) (*34*) using the CLC genomics workbench version 4.0.2 (Cambridge, MA, USA). Relevant parameters were as follows: Mismatch cost=2, Limit=10, Global alignment=True. Following the read mapping, a list of putative SNPs was created using the CLC SNP detection algorithm with the following parameters: Window length=11, Maximum gaps and mismatches=4, Minimum coverage=3, Minimum variant frequency=35%. Every SNP on this list was then investigated to ensure that the SNP was not called due to an alignment failure, and that the mutation was not present in the ancestral CM702 strain, allowing us to identify 2 SNPs that arose during the evolution experiment (see Supporting Text below).

Finding large insertions, deletions and rearrangements with de novo *assemblies*

In order to search for other mutations affecting the genome, we generated *de novo* assemblies of the CM1145 genome using the CLC genomics workbench version 4.0.2 (Relevant parameters as follows: Mismatch cost=2, Limit=10, Global Alignment=True, Non-specific matches=Randomly assigned, Conflict Resolution=Vote). We then used megablast to verify that every contig had a perfect contiguous match to the reference genome. For each contig, if the single best contiguous megablast match to the genome left 20 or more bases unaccounted for at either end of the match, we further investigated the genomic location to determine if a true mutation was present, such as an insertion sequence (IS), or if the mismatch was due to some other cause (*e.g.*, misassembly, previously known genetic manipulation, etc.).

Mutation detection by k-mer counting

The previously described mutation finding techniques are all specifically designed to detect particular mutational types (SNPs, INDELS, or novel DNA), and under certain conditions can fail to detect newly arising mutations. For example, the repetitive sequences in IS elements means that they are often difficult to assemble into unique contigs, making finding ISs from *de novo* assemblies difficult. Similarly, SNP detection against a reference genome is very sensitive to the ability of an aligner to

correctly position a mismatched basepair, and SNP calling software can fail to identify SNPs depending on the nature of the alignment or parameter settings.

Because of the above issues, we also employed an alignment-independent k-mer counting strategy to find any additional mutations that may have occurred in the CM1145 genome. Briefly, this method counts the number of times each 20 basepair long k-mer in the reference genome occurs in the 36 bp Illumina reads generated for the sequenced strain, and generates a list of all genomic locations whose kmers are not present in the sequence data. A word size of 20 basepairs was chosen because if genomic sequences were random strings of basepairs, the odds of a specific 20 k-mer occurring multiple times in the genome is vanishingly small, and as a result 95.4% of the genome (that genomic sequence not composed of repetitive sequence elements) can be uniquely identified with k-mers of this size.

Additionally, because only 0.11% of all words within a Hamming distance of 1 from any unique k-mer in the genome match another k-mer already present in the genome, sequencing errors are unlikely to lead to a false positive result that would prevent the detection of a genomic mutation. This protocol is thus able to robustly detect any mutational event in the large majority of positions in the genome.

For every block of positions in the genome whose k-mers were not represented in the sequencing data, we investigated the genomic region in the alignment of the reads to the reference as well as in the *de novo* assemblies. In all cases we could attribute the lack of k-mers to either a mutational event or to low coverage and/or erroneous sequence that could be safely ignored once reads were considered jointly. In addition to identifying all of the mutations found with the early methods, this protocol detected two large genomic deletions. First, no unique coverage was found for the smallest (~25 kb) plasmid in the reference genome (p3META1, CP001514.1) indicating that it had been completely lost in the evolved lineage. Second, the coverage of the megaplasmid META2 indicated that a large portion (~617 kb) of the genome had been deleted (fig. S7). Unique coverage for this element began from one copy of ISMex5 located at basepairs 211,853-213,135 to another copy at basepairs 855,329-856,611. Given this coverage pattern, as well as PCR verification, we infer a recombination event between these two elements leading to loss of the region without the genes encoding for replication.

Details of the benefit-cost model

It is known that the cost of protein production slows down the growth rate in *E. coli (17, 35-37)*. We observed a similar growth burden induced by expression of the foreign GSH-dependent formaldehyde oxidation pathway in *Methylobacterium* (either WT or EM). This growth burden is captured in our model with a negative fitness component (cost, c_0), that is subtracted from the unburdened fitness (or benefit, b_0). In our study, the fitness of a genotype refers to the ratio of the amortized growth rates for that strain to its competitor over the growth conditions specified. Consequently, the fitness of the ancestor (W_0), where no beneficial allele is introduced, can be written as:

$$W_0 = b_0 - c_0 = 1 \dots\dots\dots\dots\dots\dots\dots\dots\dots\dots\dots\dots\dots\dots\dots\dots\text{(eq1)}$$

The above equation provides an inherent constraint between b_0 and c_0, such that, for example, if c_0 is known, b_0 can be immediately computed as $b_0 = c_0 + 1$.

As described in the main text, the justification for proposing to subtract the cost is the hypothesis that the sum total of costs for expressing a protein at a particular level would be approximately fixed, and thus independent from mutations that simply alter the rate of converting substrate into biomass. This formulation is identical to that used to explore evolution toward optimal enzyme expression of β–galactosidase in *E. coli* (*17*). An alternative hypothesis that we considered was to treat fitness as the ratio of benefits to costs. This would imply that the same level of protein expression would impose a more (or less) cost when the strain grows faster (or slower) due to changes independent of the cost itself. This would result in a proportional 'tax' rather than a fixed 'cost'. Recent work has shown that, although the cost of a given amount of protein is not strictly constant, the proposition of simply imposing a proportional tax is refuted by the data (*38*). A proportional tax model additionally makes the prediction that there should be no epistasis observed for any mutational combinations, which contradicts the data we present (Figs. 1, 3, S9).

The fitness of a single mutant, where a single allele i is introduced into the ancestral background, is defined by the mutational effect of allele i on the benefit b_0 and on the cost c_0 with multiplicative factors λ_i and θ_i respectively. Hence fitness of this mutant (W_i) can be written as:

$$W_i = \lambda_i b_0 - \theta_i c_0 \dots\dots\dots\dots\dots\dots\dots\dots\dots\dots\dots\dots\dots\dots\dots\dots(eq2)$$

This provides allele i with two non-mutually exclusive mechanisms to improve fitness: (i) increasing the metabolic benefit ($\lambda_i > 1$) or (ii) reducing the protein cost ($\theta_i < 1$). Conversely there are two ways to decrease fitness: (i) decreasing the benefit ($\lambda_i < 1$) or (ii) increasing the cost ($\theta_i > 1$). As fitness is thus the sum of these two effects, a beneficial mutation will be any combination of values that satisfy the following:

$$W_i = \lambda_i b_0 - \theta_i c_0 > 1 \dots\dots\dots\dots\dots\dots\dots\dots\dots\dots\dots\dots\dots\dots\dots(eq3)$$

When considering double mutants, we propose that every mutation affects each *component* of the fitness (b_0 and c_0) independently of previous mutations, giving rise to a multiplicative accumulation of effects for each term, as follows:

$$W_{ij} = \lambda_i \lambda_j b_0 - \theta_i \theta_j c_0 \dots\dots\dots\dots\dots\dots\dots\dots\dots\dots\dots\dots\dots\dots(eq4)$$

A generalized version of the above equation is then hypothesized to describe the fitness of any multiallele mutant:

$$W_{i_1 .. i_n} = \prod_{i=i_1}^{i_n} \lambda_i b_0 - \prod_{i=i_1}^{i_n} \theta_i c_0 \dots\dots\dots\dots\dots\dots\dots\dots\dots\dots\dots\dots(eq5)$$

Consequently, our formulation of fitness provides a putative way of predicting the fitness of any multiallele combination from the knowledge of c_0 (with $b_0 = 1 + c_0$ automatically determined) and of the multiplicative factor λ_i and θ_i for each single allele i.

Estimating parameters of the benefit-cost model

The parameters of our model were determined through a series of experimental observations. Since expression cannot be eliminated entirely in EM to cleanly estimate c_0 in that genotype, we use the fitness advantage of removing expression in WT to provide an estimate for $c_0 = 0.141$, and thus $b_0 = c_0 + W_0 = 0.141 + 1 = 1.141$.

Next, we utilize the experimental data to estimate the parameters θ, describing the change in cost induced by each individual mutation. Given the link between fitness change and cell morphology abnormality discussed in the main text (Fig. 1), we assume that the cost change factor θ_i induced by mutation i is related to the percentage of the abnormal cells found in that population. The intuition here is that although the burden felt from expressing the foreign pathway can be considered on a continuous scale, it appears to manifest as discrete phenotypes, suggesting that there may be a threshold behavior for this morphological phenotype (*e.g.*, cells were either branched, or not branched). This may be an analogous scenario to induction of the lactose operon, where a continuous change in inducer concentration shifts a genetically identical population from being all off, to some on and some off, to all on (rather than the alternative of a graded response with a unimodal distribution at moderate inducer concentrations) (*36*). This proxy is of course very much an approximate hypothesis of what may be occurring. Reassuringly, cell length - another possible proxy - tracks well with this proportion. Furthermore, changes in relative cell length (as estimated by flow cytometry) provide two further confirmations of our proposed model. First, combinations of "cost-reducer" mutations lead to continuing decreases in cell length (fig. S2H). Second, all populations show the trend of reduction in cell size in the first 300 generations of the experiment (fig. S2D). It should be noted, however, that the visual manifestation of this cost appears to be less in the WT strain that does not grow as poorly as the EM strain.

Given this, we estimate θ_i for a beneficial allele i that is proportional to the relative proportion of abnormal cells compared to the EM ancestor, i.e.:

$$\theta_i = p_i / p_0 \dots\dots\dots\dots\dots\dots\dots\dots\dots\dots\dots\dots\dots\dots\dots\dots(eq6)$$

Here p_0 and p_i are the proportion of the abnormal cells in the population of ancestor and single mutant strain i, respectively. By rearranging (eq2), λ_i can be written as the follows:

$$\lambda_i = (W_i + \theta_i c_0) / b_0 \quad\ldots\ldots\ldots\ldots\ldots\ldots\ldots\ldots\ldots\ldots\ldots\ldots\ldots\ldots\ldots\ldots\text{(eq7)}$$

Using our estimated parameters c_0 and θ_i, we can then calculate an estimated λ_i for each single mutant strain i (table S3). Once these parameters were determined from single allele data, we can apply (eq5) to predict all the fitness of multi-allele strains (fig. S9B). Compared with the standard "no epistasis" model that lacks a cost component (fig. S8A), our benefit-cost model obtains a much better agreement with the data. In addition, the residual plot for the standard model and the benefit-cost model indicates that the benefit-cost model (residuals are randomly distributed) is an appropriate estimate for the multi-allele fitness while the standard model is not since a clear trend of residuals exist (fig. S10).

Supporting Text

Comparisons of alternative formulations for genetic interactions

In this work, we quantify epistatic interactions relative to a baseline that is the most commonly used null model in evolutionary genetics (*1, 2*). This null model assumes that mutations that alter a given phenotype do so to the same proportional extent on any genetic background. There is some understandable confusion about naming conventions, as this model is sometimes called 'additive' due to its constant effect on log-transformed phenotype, but has mostly been labeled as 'multiplicative'. A formulation that gives strict additivity is a simple linear model which assumes each mutation adds a constant change to a phenotype, a definition of epistasis first proposed by Fisher (*39*).

Simple linear models are commonly used for inferring the effects of different genetic markers on phenotypes in quantitative genetic and genome association studies and are used in many fields for statistical inference partly due to their tractability (*1, 40*). In the context of the present study, the primary phenotype examined is fitness, which is largely determined by the growth rate of the bacterium. Our rationale for employing a multiplicative model is two-fold: First, it is hard to imagine a biological mechanism by which a genetic perturbation could confer a constant absolute effect on the growth rate that is independent of the growth rate of the unperturbed organism. Second, in contrast to an additive model, the multiplicative model can be sensibly interpreted in the context of our work.

We offer two examples to illuminate why a multiplicative model, in the absence of any other information about the process in question, is the expectation for independent modifiers of a phenotype. First, consider a genotype of a plant that produces a given number of seedlings. The number of seedlings could be doubled through two different mutations, one that doubles the number of seedlings, the other that doubles the probability that they germinate. Given the null expectation that these two mutations act independently on this trait, there would be a four-fold increase in seedlings for a multiplicative model. In contrast, an additive model would only suggest a three-fold increase. Second, consider a metabolic example. The activity of an enzyme in a cell could be doubled by either doubling the amount of that enzyme or the catalytic activity per molecule (*i.e.*, k_{cat}). Again, under the assumption of independence these mutations would be expected to quadruple activity.

Our data shown in Fig. 1 show a clear pattern of diminishing proportional return for most mutations upon fitter backgrounds. It can be noted that the absolute increases in fitness conferred by each allele ($W_{1,background} - W_{0,background}$, where 1 and 0 indicate the presence of the evolved and wildtype alleles, respectively) are, in fact, reasonably close to being a constant across the eight different backgrounds on which they were tested. Paradoxically, this implies that the observed diminishing returns trend may comply with the null expectation relative to an additive model. In contrast, relative to the physiologically interpretable multiplicative model the data represent a departure from the null expectation of a constant proportional effect.

Mutations that arose during the evolution experiment in the EVO strain

Only 9 of the mutations that distinguish the EVO strain (CM1145) from the reference genome available in GenBank (*34*) occurred during evolution to methanol. There were 15 additional differences identified that were preexisting in the EM ancestor of the F4 population (CM702). Three of these were simply the known manipulations to generate CM702: $\Delta mptG$, $crtI^{502}$, pCM410 (described above). Eleven

further differences were already present in our WT isolate (*i.e.*, CM501). These included eight small indels (in the main chromosome META1: +C, 482895; ΔG, 2329711; ΔC, 3037770; ΔG, 3159071; ΔCGTGC, 4000779; +CCGTG, 4001535; on the megaplasmid META2: +C, 580985; ΔG, 770864) and three SNPs (on META1: T→G, 2777457; C→T, 2803789; T→C, 2803840). These may represent either sequencing errors in the reference (or less likely, both sets of Illumina data here) or actual differences between CM501 and the isolate used to generate the gDNA for the reference genome. A final mutation was identified in EVO that was missing in WT, yet was already present in the EM ancestor. This change, a 12 bp deletion (ΔGCCGCCGCGGAC, 3844018 of META1) in META1_3695, shortens this hypothetical protein that is a putative "lytic transglycosylase, catalytic" by 4 amino acids (removes Ala-Ala-Asp-Ala). This mutation was confirmed via PCR and sequencing, and thus apparently arose at some point during the construction of the EM strain (CM501→S234-13→CM502→CM624→CM702; see above and Table S2).

The following 9 mutational events were identified in EVO but in neither the EM ancestor nor WT, and thus emerged during the course of the 600 generations of adaptation to methanol. For the purposes of this paper, mutations A through C correspond to loci 1 through 3, while mutations D through I are collectively treated as the fourth locus, "*GB*" (*genetic background*).

Mutation A - 11 bp deletion in 326 **the introduced plasmid (*fghA*^{1145}, or here *fghA*^{EVO})**

This is a deletion of the sequence "AGGGAAGAACC" that occurs at position 3,790 in the introduced plasmid. This deletion occurs between the *flha* and *fghA* genes and is described in the main text.

Mutation B - SNP in the chromosome (*pntAB*^{1145}, or here *pntAB*^{EVO})

This mutation is a C->T substitution that occurs at position 3,087,664 in the chromosome. This mutation occurs 48 bp upstream of the pyridine nucleotide transhydrogenase gene (*pntAB*).

Mutation C - 2 bp deletion in the chromosome (*gshA*^{1145}, or here *gshA*^{EVO})

A 2 bp deletion occurred at position 701,477 in the promoter region (127 bp upstream of the start codon) of the most rate-limiting enzyme of GSH biosynthesis, γ-glutamylcysteine synthetase (*gshA*).

Mutation D - IS insertion into the chromosome

An insertion sequence, ISMex4 (*34*), inserted at approximately position 1,122,226 in the META1 chromosome. This insertion results in the ~50X up-regulation of a cobalt transport cassette (allele = *icuAB*^{1145}) and has been extensively characterized in previous work (*15*). Although beneficial in metal-poor medium, this locus was not treated separately here due to being neutral in metal replete medium (*15*).

Mutation E - SNP in the megaplasmid

This mutation is a C->T substitution that occurs at position 372,544 in the megaplasmid. The mutation is a synonymous substitution in the coding sequence annotated as META2_0422. This protein has no homology to any previously reported protein.

Mutation F - IS insertion into the chromosome

The insertion sequence ISMex2 (*34*) inserted itself at approximately position 2,860,154. This mutation occurs in between the two proteins *ccmC* and *ccmD.* These proteins in *E. coli* are part of the type 1 cytochrome *c* biogenesis complex and are involved in transporting heme from the cytoplasm to the periplasm, where it can then be incoporated into cytochrome *c* apoproteins (*41*).

Mutation G: Small insertion in chromosome

This is an insertion of 6 bp into the conserved hypothetical protein annotated as META1_4902. The mutation occurs at position 5,022,190. This insertion keeps the protein in frame, and introduces 2 additional amino acids which are a copy of the preceding two in the protein.

Mutation H – Large deletion in the megaplasmid

A presumed recombination event between homologous transposases annotated as part of the ISMex5 family (*34*) resulted in a large deletion on the megaplasmid (fig. S7). The recombination event occurred between the genes that occurred in position 211,853-213,135 and the one from 855,329-856,611.

Mutation I - Loss of plasmid p3META

The smallest plasmid present in the reference genome was lost during the evolution experiment. The plasmid is 25 kb in size and contains 35 genes (~0.5% of the total genes in the reference genome).

Connection of the products of* fghA*,* pntAB *and* gshA *to the engineered C$_1$ metabolism in the EM strain

The three identified mutations which we have considered as individual loci have direct connections to the modified C$_1$ metabolism in the EM strain following inactivation of the tetrahydromethanopterin dependent pathway for the GSH-dependent one. The first is obvious: *fghA (*and *flhA* upstream of it*)* encode the second of the two enzymes of the introduced pathway (formyl-GSH hydrolase and hydroxymethyl-GSH dehydrogenase) (*28, 29*). The *fghA^{EVO}* allele reduces expression of both genes in the introduced pathway (see main text). The second mutation is upstream of *pntAB*, which encodes transhydrogenase. This enzyme inter-converts $NADH + NADP^+ + H^+_p \rightarrow NAD^+ + NADPH + H^+_c$ (where H^+_p and H^+_c represent periplasmic and cytoplasmic protons, respectively). Whereas the original H$_4$MPT pathway could couple to either NADH or NADPH, FlhA of the GSH pathway only acts to generate NADH. This removes the only known direct route for NADPH synthesis for assimilation reactions, making transhydrogenase critical for growth. This mutation therefore likely helps increase the cell's capacity to generate NADPH. The third mutation is upstream of *gshA*, encoding γ-glutamylcysteine synthetase. The new pathway requires GSH as the C$_1$-carrier, yet GSH is involved in myriad cellular functions involving redox balance and removal of toxic compounds. As such, if this mutation increases the cellular pool of GSH it may alleviate the limitation for this compound in general cellular functions. Furthermore, it is notable that the reaction of formaldehyde with GSH is non-enzymatic in EM. This is in contrast to *Paracoccus denitrificans*, where the pathway was cloned from. It was found that *P. denitrificans* makes a novel enzyme (GFA, a GSH dependent formaldehyde-activating enzyme) (*42*) that catalyzes this reaction. Thus, another key benefit that could come from elevated GSH concentrations would be an increased rate of reaction with formaldehyde.

Sensitivity analyses of the benefit-cost model

In fig. S9 we test how well our model can predict fitness of multi-allele strains by calculating the sum of square error (Σ) for the fitness between data and our model.

$$\Sigma = \sum_i \left(W_i^{data} - W_i^{model} \right)^2 \quad \text{...(eq8)}$$

As we can search for an optimal c_0 best predicts the fitness of multi-allele strains (fig. S9C-D), one might ask whether the remarkably good prediction of experimentally derived fitness can be achieved by chance. Could our model always find a c_0 that will give comparable predictions for random datasets? To address this issue, we test the null hypothesis that our model can always perform as well as it predicts the fitness for real data. We calculate the p-value for the model to obtain a better sum of square error (less than 0.0134, the one obtained with the measured $c_0=0.141$) in a permuted data generated by shuffling double and triple mutants 1,000,000 times (out of 10! sample space). The p-value we obtain from this permutation test is 0.00005, indicating that it is highly unlikely for the model to achieve such a good prediction by chance.

Alternatively, randomly generating 1,000,000 single peaked fitness landscapes using a rejection sampling scheme that simulated fitnesses for the double and triple mutants confirms that the accuracy for prediction cannot be achieved in these random trajectories (none of the random trajectories achieve a better sum of square error). Fitness landscapes were proposed by drawing the value of the double and triple mutants from uniform distributions ranging from the value of the highest observed single mutant fitness to the highest observed fitness of a genotype with one additional mutation relative to the genotype being simulated. Only simulations resulting in single peaked landscapes were considered.

Using a slightly different approach, it is interesting to ask how the comparison between data and model would change for different values of c_0. In addition to allowing us to perform a sensitivity analysis relative to c_0, this calculation will show us whether there is a c_0 that gives optimal agreement between data and model (and how close this optimal c_0 is to the experimentally estimated one), and how the model

behaves as it approaches the c_0=0 condition, which corresponds to a standard definition of non-epistatically interacting mutations. Hence, treating c_0 as a free parameter, we can search for the optimal c_0 that minimize the sum of square error Σ. The sensitivity analysis indicates two messages for the model:

(1) Measured c_0 is quite close to the optimal c_0

A sensitivity analysis on c_0 shows that the choice of c_0=0.141 approximated from the experiment provides a similar quality of fitness prediction, compared with the optimal c_0=0.119 (fig. S9C). In addition, the results indicate that the model is not particularly sensitive to the choice of c_0 as a wide range of c_0 produce comparable sum of square error between the model and data.

(2) Both benefit and cost components are required for the model

As expected from the sensitivity analysis, when c_0 approaches zero, data and model disagree quite significantly relative to the optimum, indicating the term c_0 is necessary to capture the antagonism at the fitness level, under the multiplicative rule of how alleles combine. On the other hand, a cost-only formulation ($b_0 = 0$, indicating the only way to improve fitness is by cutting the cost) is not tenable because $pntAB^{EVO}$ barely reduces costs ($\theta \cong 1$), such that it would be predicted to be a neutral mutation. Therefore, both the cost and benefit term c_0 and b_0 are necessary as the minimal model to recapitulate the fitness of multi-allele strains and the antagonistic pattern we observe.
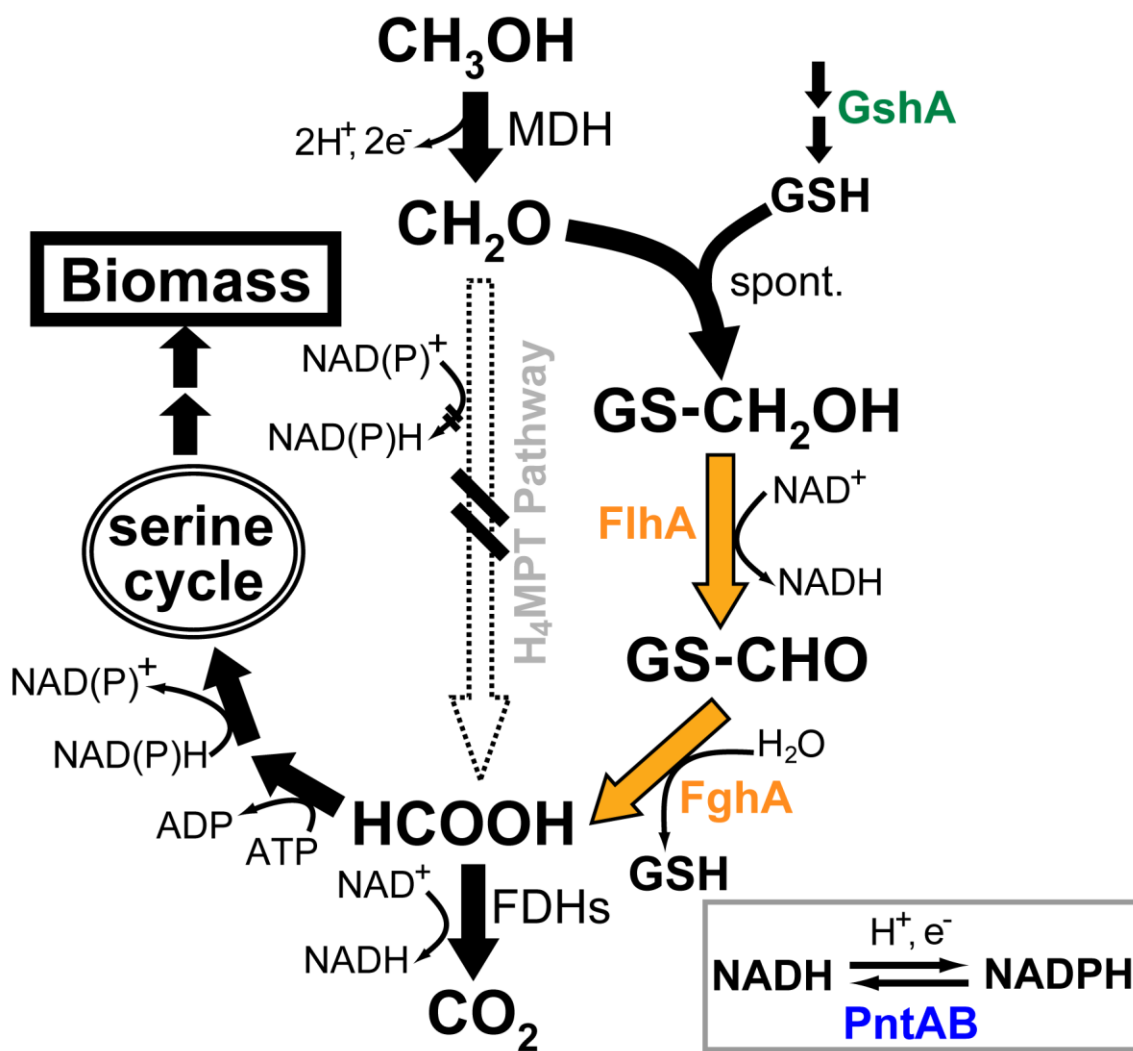
Figure S1. C_1 network in EM ancestor. Methanol (CH_3OH) is first oxidized to formaldehyde (CH_2O) via methanol dehydrogenase (MDH). CH_2O can then react spontaneously with GSH (biosynthesis of which depends upon the gene product of *gshA*, γ-glutamylcysteine synthetase; indicated in green) to form hydroxymethyl-GSH (GS-CH_2OH). This is oxidized to formyl-GSH (GSH-CHO) by the first introduced gene product, NAD-dependent GS-CH_2OH dehydrogenase (encoded by *flhA*), creating NADH in the process. The formyl group is then hydrolyzed to formate (HCOOH) by the second introduced enzyme, GS-CHO hydrolase (encoded by *fghA*; both are indicated here in yellow). HCOOH is subsequently oxidized to CO_2 via one of several formate dehydrogenases (FDHs) or is assimilated into biomass via a series of tetrahydrofolate-dependent reactions in order to enter into the serine cycle to be assimilated into multi-C compounds. The reaction inter-converting NADH (and $NADP^+$) to NADPH (and NAD^+; at the cost of one H^+ translocated across the cytoplasmic membrane) which is catalyzed by transhydrogenase (encoded by *pntAB*; indicated in blue) is also indicated. The new GSH-dependent pathway only generates NADH directly, whereas the endogenous tetrahydromethanopterin (H_4MPT)-dependent pathway that was disabled (shown in grey and crossed out) in the EM strain can generate either NADH or NADPH.
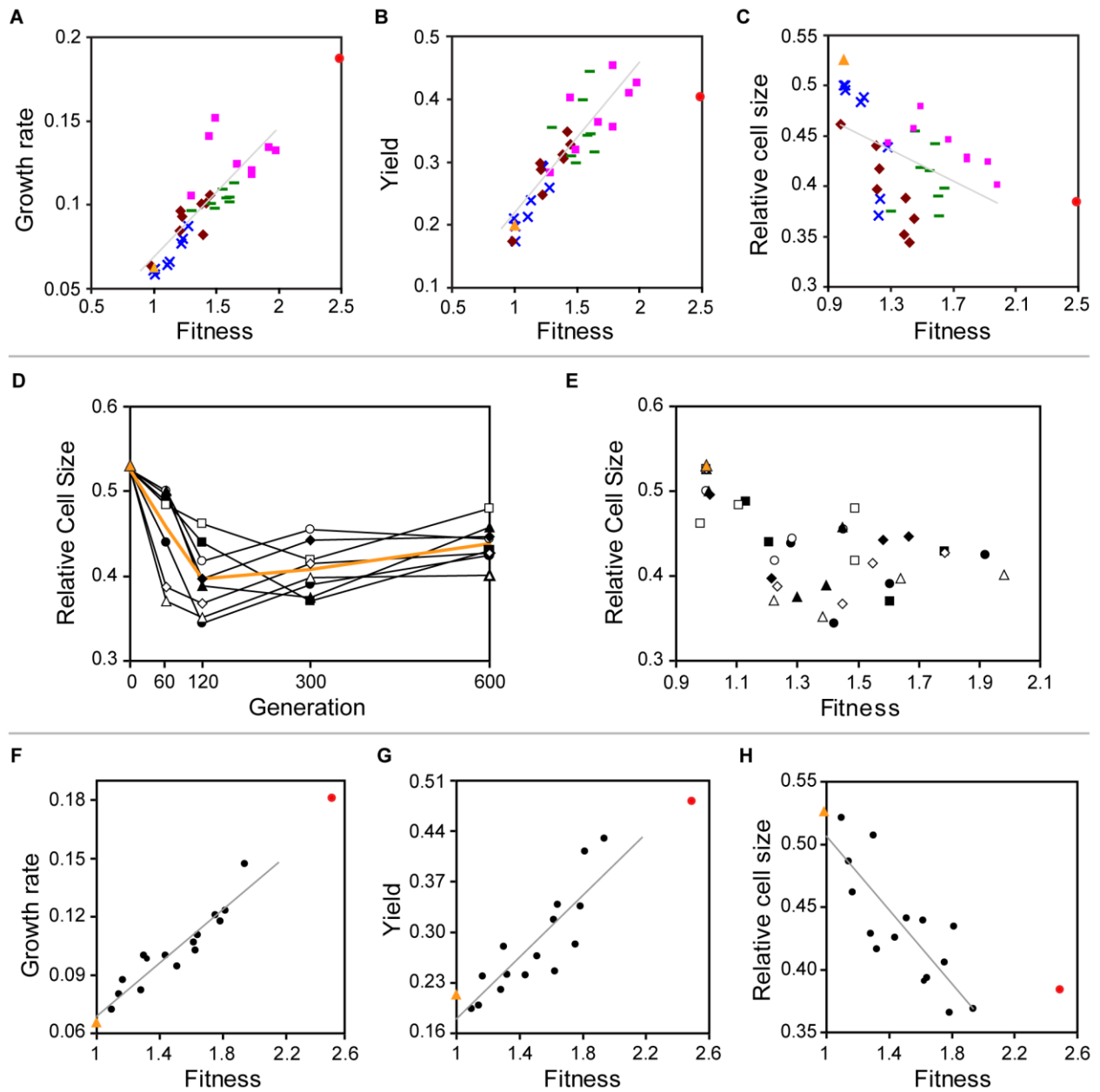
Figure S2. – Fitness vs. rate, yield or cell size. In all panels: WT, red circle; EM, orange triangle; regression lines, grey. Panels **A**, **B**, **C**: isolates from generation 60 (blue crosses), 120 (brown diamonds), 300 (green dashes), 600 (purple squares). Panels **D**, **E**: isolates from F1 through F8 (●, ○, ▲, △, ■, □, ◆, ◇); grand mean of relative cell size, orange line. Panels **F**, **G**, **H**: strains with evolved allele combinations, black dots.
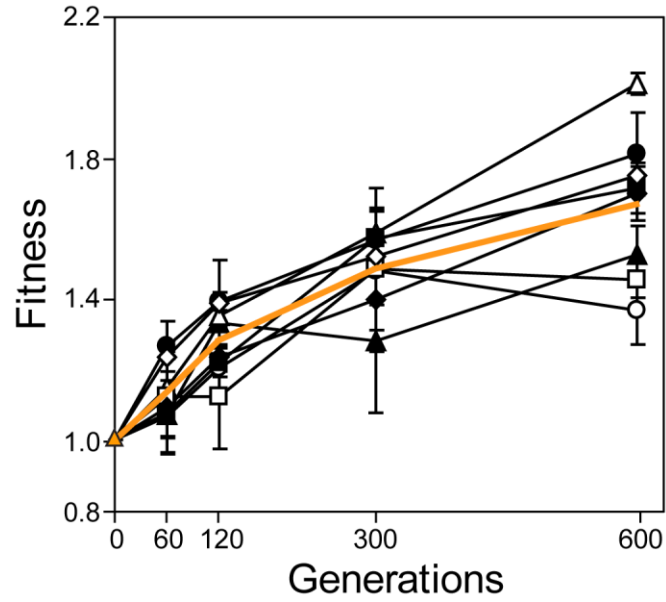
Figure S3. Dynamics of adaptation of the EM strain evolved in medium containing methanol. Fitness increases through time for replicate populations F1 through F8 (●, ○, ▲, △, ■, □, ◆, ◇). Orange triangles and line indicate the EM strain and the grand population mean, respectively.
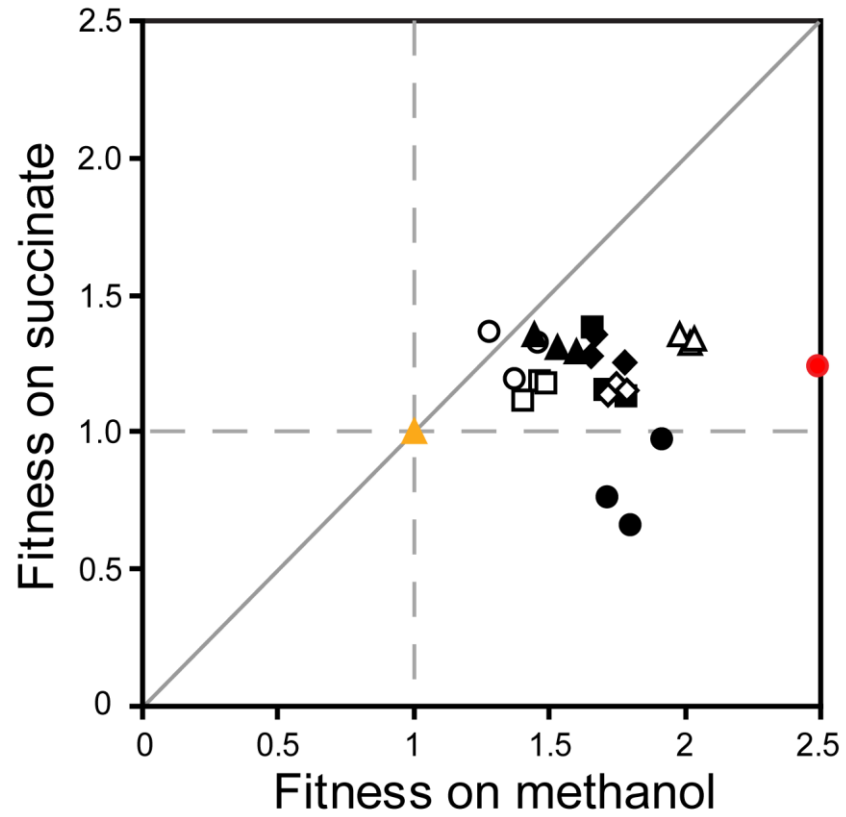
Figure S4. Fitness on methanol vs. succinate. WT, red circle; EM, orange triangle; three evolved isolates from each of F1 through F8 after 600 generations in methanol ($\bullet$, $\circ$, $\blacktriangle$, $\triangle$, $\blacksquare$, $\square$, $\blacklozenge$, $\lozenge$).
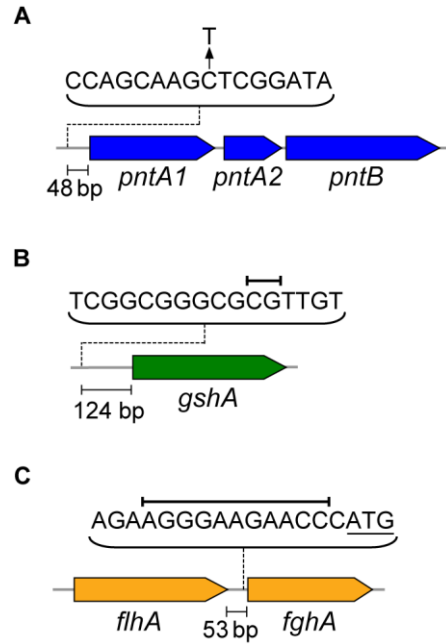
Figure S5. Three focal mutations related to C_1 metabolism. Details of the genetic changes and relationship to methylotrophy in the EM strain are discussed above in Supplemental Text.
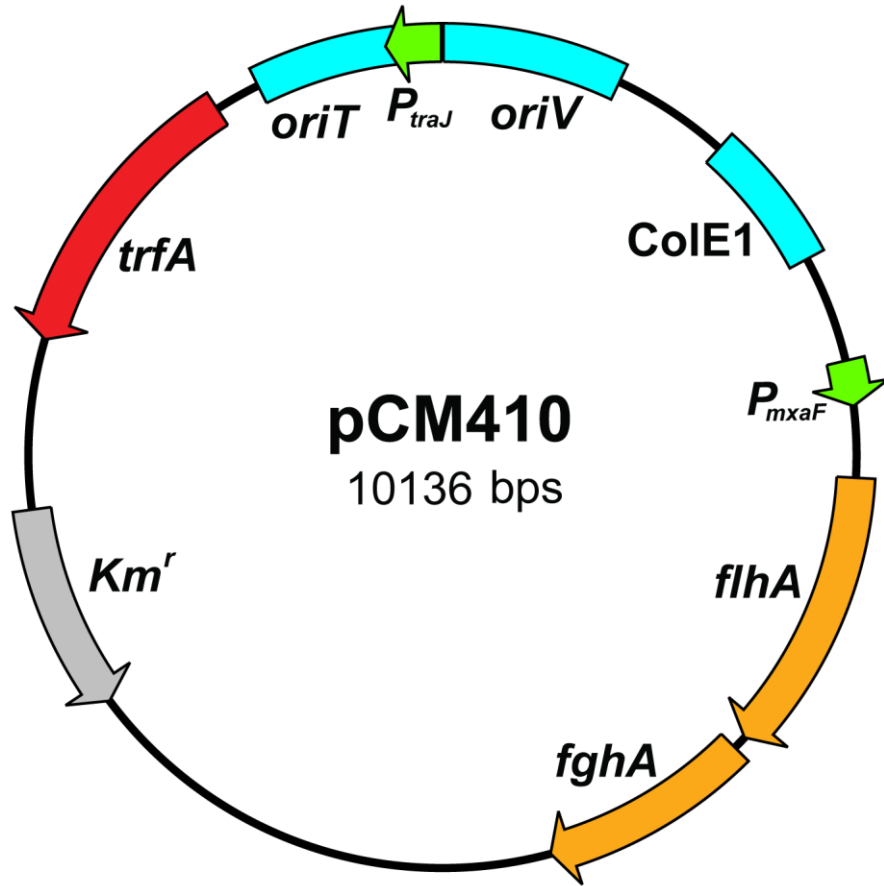
Figure S6. The physical map of the pCM410 plasmid (GenBank accession no. FJ389188). P_{mxaF}, strong, endogenous methanol dehydrogenase promoter; *flhA* and *fghA*, enzymes of the introduced GSH dependent formaldehyde oxidation pathway; *trfA*, plasmid replication initiator gene; *oriV*, IncP origin of replication; *oriT*, origin of transfer; *colE1*, high-copy origin of replication in *E. coli*; Km^r, kanamycin resistance marker.
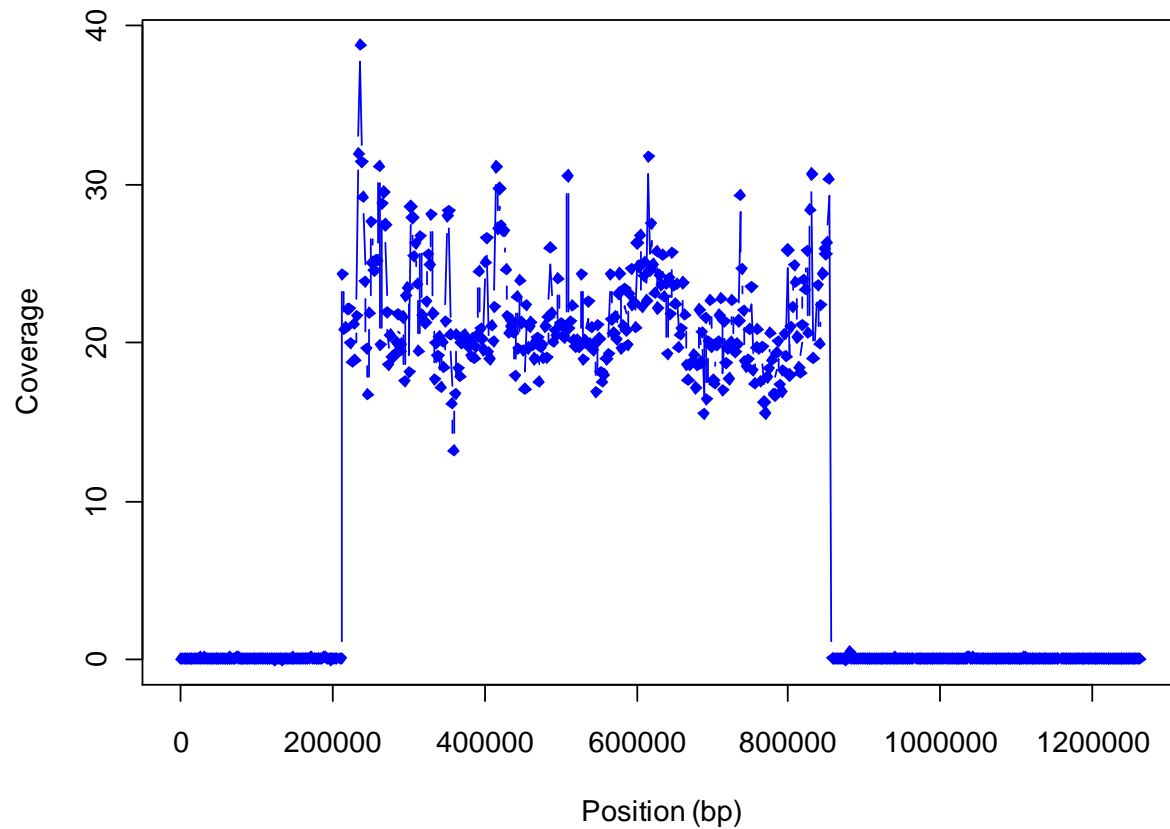
Figure S7. The mean frequency of k-mers that uniquely occur only in the genome along the length of the META2 megaplasmid (binned in 2000 bp windows). Unique coverage appears for the middle of the chromosome, but is absent on either side at the location of a copy of ISMex5 (*34*) as a result of a deletion. Given that META2 is circular, this indicates that a ~617 kb region was deleted, leaving only the undeleted sections of the megaplasmid.

Figure S8. Distribution of cell lengths for WT (white) and EM (black).
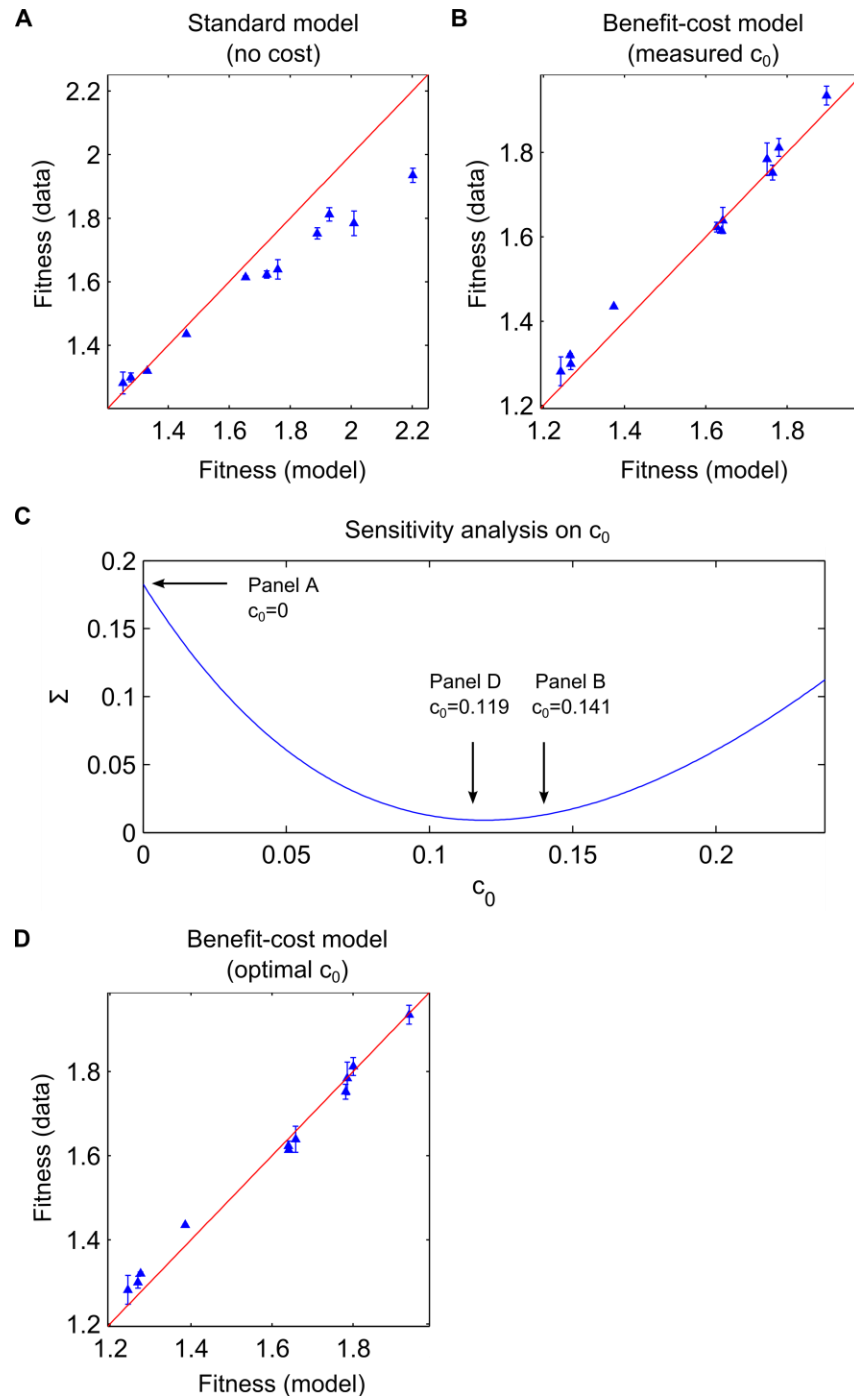
Figure S9. Goodness of fit and sensitivity analysis of the model. Error bar represents the standard error of three replicates. (**A**) Plot of fitness values for the 11 mutation combinations versus those predicted from the standard model (using $c_0 = 0$, the benefit-cost model will be equivalent to the standard model correspond to 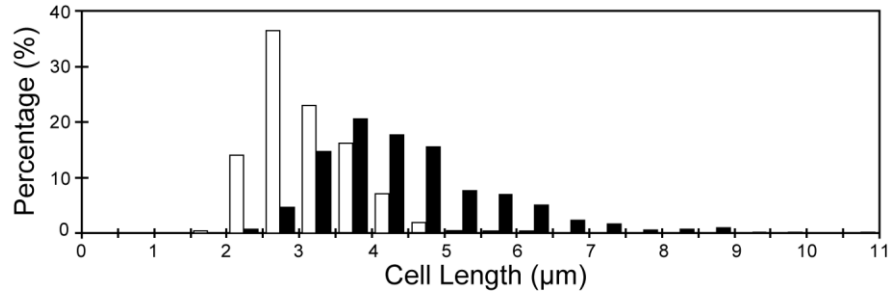standard model $W_{i,background} = W_i W_{background}$). The straight line represents the perfect prediction. (**B**) Comparison of predictions and experimental data, as done in (**A**), using the benefit-cost model ($W_{mutant} = \Pi\lambda_i b_0 - \Pi\theta_i c_0$) with experimentally determined $c_0 = 0.141$. (**C**) Sensitivity analysis for the benefit-cost model at various choices of c_0 indicates that experimentally measured $c_0 = 0.141$ (A) provides a similar quality of fitness prediction to the optimal $c_0 = 0.119$ (D) with sum of square error $\Sigma=0.0134$ and 0.0091, respectively. (**D**) The best fit of the benefit-cost model with optimal $c_0 = 0.119$.
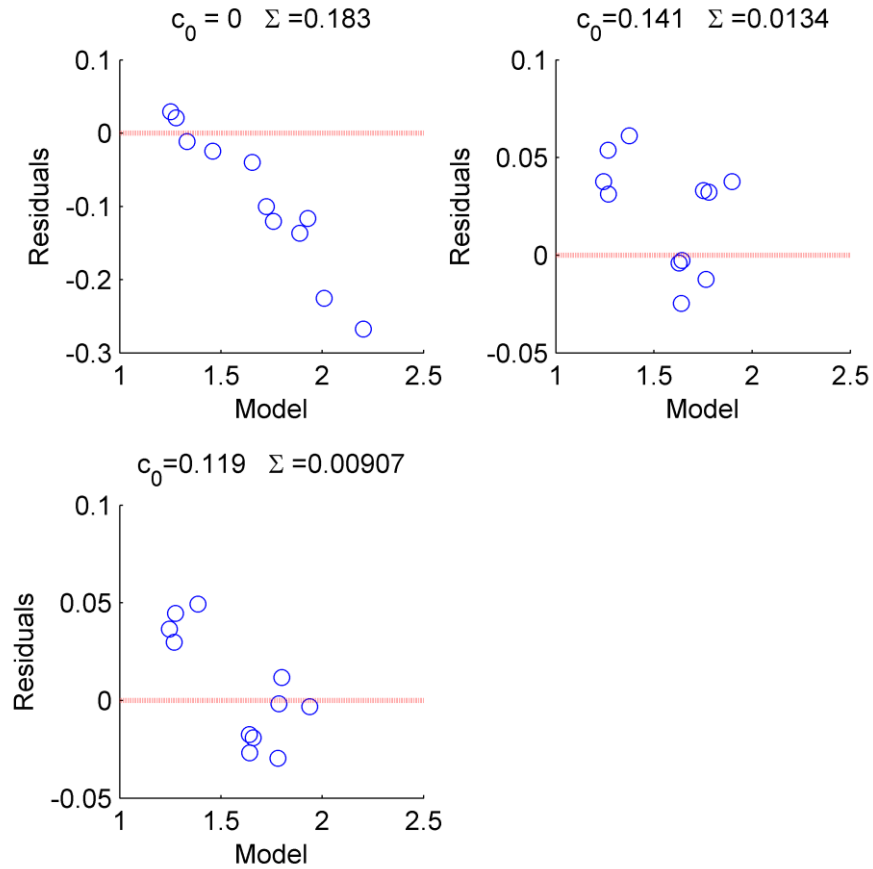
Figure S10. Residual plot for the standard model and the benefit-cost model. (**A**) The standard model is not a good estimate for fitness since the residuals (measured fitness – predicted fitness) show a clear pattern that is not randomly dispersed around zero. (**B**) (**C**) The benefit-cost model not only shows smaller residuals, but also do not show any clear trends, indicating the prediction made by the benefit-cost model is appropriate.

Table S1. Fitness and cell size of evolved isolates

Strain	Population	Generation	Fitness	*Relative cell size
CM911	F1	60	1.252 ± 0.013	
CM912	F1	60	1.270 ± 0.013	
CM913	F1	60	1.279 ± 0.065	0.439
CM914	F2	60	1.035 ± 0.017	
CM915	F2	60	1.169 ± 0.007	
CM916	F2	60	0.998 ± 0.016	0.501
CM917	F3	60	1.105 ± 0.014	
CM918	F3	60	1.007 ± 0.020	0.501
CM919	F3	60	1.111 ± 0.023	
CM920	F4	60	1.272 ± 0.012	
CM921	F4	60	1.220 ± 0.008	0.371
CM922	F4	60	0.958 ± 0.039	
CM923	F5	60	1.101 ± 0.036	
CM924	F5	60	1.129 ± 0.032	0.488
CM925	F5	60	1.009 ± 0.010	
CM926	F6	60	1.108 ± 0.035	0.484
CM927	F6	60	1.076 ± 0.013	
CM928	F6	60	1.196 ± 0.031	
CM929	F7	60	1.133 ± 0.022	
CM930	F7	60	1.135 ± 0.041	
CM931	F7	60	1.011 ± 0.037	0.496
CM932	F8	60	1.237 ± 0.025	
CM933	F8	60	1.232 ± 0.016	0.387
CM934	F8	60	1.242 ± 0.010	
CM935	F1	120	1.420 ± 0.010	0.344
CM936	F1	120	1.391 ± 0.045	
CM937	F1	120	1.374 ± 0.062	
CM938	F2	120	1.181 ± 0.009	
CM939	F2	120	1.216 ± 0.048	
CM940	F2	120	1.225 ± 0.032	0.417
CM941	F3	120	1.312 ± 0.071	
CM942	F3	120	1.289 ± 0.010	
CM943	F3	120	1.394 ± 0.007	0.388
CM944	F4	120	1.324 ± 0.040	
CM945	F4	120	1.357 ± 0.060	
CM946	F4	120	1.384 ± 0.014	0.352
CM947	F5	120	1.212 ± 0.050	
CM948	F5	120	1.206 ± 0.010	0.440
CM949	F5	120	1.244 ± 0.005	
CM950	F6	120	1.171 ± 0.031	
CM951	F6	120	0.980 ± 0.042	0.462

CM952	F6	120	1.229 ± 0.033	
CM953	F7	120	1.252 ± 0.065	
CM954	F7	120	1.214 ± 0.011	0.397
CM955	F7	120	1.246 ± 0.006	
CM956	F8	120	1.449 ± 0.061	0.368
CM957	F8	120	1.454 ± 0.008	
CM958	F8	120	1.268 ± 0.006	
CM1145	**F4**	**600**	**1.935 ± 0.062**	**0.426**
CM1606	F1	300	1.604 ± 0.013	0.390
CM1607	F1	300	1.487 ± 0.052	
CM1608	F1	300	1.615 ± 0.055	
CM1609	F2	300	1.413 ± 0.066	
CM1610	F2	300	1.577 ± 0.021	
CM1611	F2	300	1.454 ± 0.017	0.455
CM1612	F3	300	1.254 ± 0.021	
CM1613	F3	300	1.300 ± 0.061	0.375
CM1614	F3	300	1.294 ± 0.024	
CM1615	F4	300	1.641 ± 0.036	0.398
CM1616	F4	300	1.596 ± 0.019	
CM1617	F4	300	1.527 ± 0.028	
CM1618	F5	300	1.626 ± 0.019	
CM1619	F5	300	1.480 ± 0.032	
CM1620	F5	300	1.607 ± 0.026	0.370
CM1621	F6	300	1.481 ± 0.072	
CM1622	F6	300	1.491 ± 0.020	0.418
CM1623	F6	300	1.484 ± 0.024	
CM1624	F7	300	1.537 ± 0.013	
CM1625	F7	300	1.583 ± 0.012	0.442
CM1626	F7	300	1.075 ± 0.032	
CM1627	F8	300	1.471 ± 0.010	
CM1628	F8	300	1.549 ± 0.019	0.415
CM1629	F8	300	1.545 ± 0.055	
CM1726	F1	600	1.921 ± 0.047	0.425
CM1727	F1	600	1.805 ± 0.019	
CM1728	F1	600	1.718 ± 0.025	
CM1729	F2	600	1.373 ± 0.010	
CM1730	F2	600	1.459 ± 0.020	
CM1731	F2	600	1.284 ± 0.056	0.444
CM1732	F3	600	1.597 ± 0.021	
CM1733	F3	600	1.447 ± 0.018	0.458
CM1734	F3	600	1.531 ± 0.022	
CM1735	F4	600	2.019 ± 0.091	
CM1736	F4	600	1.981 ± 0.087	0.401
CM1737	F4	600	2.035 ± 0.063	

CM1738	F5	600	1.786 ± 0.070	0.429
CM1739	F5	600	1.706 ± 0.062	
CM1740	F5	600	1.660 ± 0.036	
CM1741	F6	600	1.471 ± 0.024	
CM1742	F6	600	1.491 ± 0.033	0.480
CM1743	F6	600	1.403 ± 0.022	
CM1744	F7	600	1.653 ± 0.047	
CM1745	F7	600	1.668 ± 0.017	0.447
CM1746	F7	600	1.777 ± 0.024	
CM1747	F8	600	1.748 ± 0.038	
CM1748	F8	600	1.716 ± 0.022	
CM1749	F8	600	1.786 ± 0.021	0.427

*Cell size of one isolate chosen randomly from each population at a given time point was measured using flow cytometry and reported as the forward scatter value.

Table S2. Bacterial strains and plasmid constructs.

Strain or plasmid	Description	Source or reference
Strains		
CM501	Pink-colored wild-type	(*23*)
CM502	White-colored wild-type (here 'WT'), $crtI^{502}$	(*23*)
CM508	$\Delta mptG$	(*23*)
CM611	$crtI^{502}$, $katA::kan$	(*27*)
CM624	$crtI^{502}$, $\Delta mptG$	This study
CM701	$\Delta mptG$, pCM410; pink engineered ancestor	This study
CM702	$crtI^{502}$, $\Delta mptG$, pCM410; white eng. ancestor (here 'EM')	This study
CM1145	Evolved isolate (here 'EVO') from F4 population at gen. 600	(*15*)
CM1175	$katA::loxP\text{-}t_{rrnB}\text{-}P_{tacA}\text{-}mCherry\text{-}t_{T7}$	(*27*)
CM1176	$crtI^{502}$, $katA::loxP\text{-}t_{rrnB}\text{-}P_{tacA}\text{-}mCherry\text{-}t_{T7}$	(*27*)
CM1180	$crtI^{502}$, $katA::loxP\text{-}t_{rrnB}\text{-}P_{tacA}\text{-}Venus\text{-}t_{T7}$	(*27*)
CM1225	$katA::loxP\text{-}t_{rrnB}\text{-}P_{tacA}\text{-}mCherry\text{-}t_{T7}$, $\Delta mptG$	This study
CM1226	$crtI^{502}$, $katA::loxP\text{-}t_{rrnB}\text{-}P_{tacA}\text{-}mCherry\text{-}t_{T7}$, $\Delta mptG$	This study
CM1231	$katA::loxP\text{-}t_{rrnB}\text{-}P_{tacA}\text{-}mCherry\text{-}t_{T7}$, $\Delta mptG$, pCM410	This study
CM1232	$crtI^{502}$, $katA::loxP\text{-}t_{rrnB}\text{-}P_{tacA}\text{-}mCherry\text{-}t_{T7}$, $\Delta mptG$, pCM410	This study
CM1275	CM624 with pCM410.1145; *strain "1000" (*i.e.*, $fghA^{EVO}$)	(*15*)
CM1276	CM1145 cured of pCM410.1145	This study
CM1277	CM1276 with pCM410; strain "0111"	This study
CM1287	CM1276 with $pntAB^{WT}$ (using pHC35)	This study
CM1290	CM624 with $pntAB^{EVO}$ (using pHC36)	This study
CM1293	CM1276 with $gshA^{WT}$ (using pHC37)	This study
CM1298	CM624 with $gshA^{EVO}$ (using pHC38)	This study
CM1310	CM1287 with pCM410; strain "0011"	This study
CM1311	CM1287 with pCM410.1145; strain "1011"	This study
CM1312	CM1290 with pCM410; strain "0100"	(*15*)
CM1313	CM1290 with pCM410.1145; strain "1100"	This study
CM1314	CM1293 with pCM410; strain "0101"	This study
CM1315	CM1293 with pCM410.1145; strain "1101"	This study
CM1316	CM1298 with pCM410; strain "0010"	(*15*)
CM1317	CM1298 with pCM410.1145; strain "1010"	This study

CM1348	CM1290 with $gshA^{EVO}$ (using pHC38)	This study
CM1350	CM1287 with $gshA^{WT}$ (using pHC37)	This study
CM1784	CM1348 with pCM410; strain "0110"	This study
CM1785	CM1348 with pCM410.1145; strain "1110"	This study
CM1786	CM1350 with pCM410; strain "0001"	This study
CM1787	CM1350 with pCM410.1145; strain "1001"	This study
S234-13	*crtI*::IS*phoA/hah*-Tc; transposon mutant used to make CM502	(*22*)

Plasmids

pCM106	P_{mxaF}-*flhA*-*fghA*; †Tc^r	(*14*)
pCM157	*cre*-expression vector; Tc^r	(*25*)
pCM160	P_{mxaF} expression vector; ‡Km^r	(*26*)
pCM253	*cre-lox* allelic exchange plasmid with a Δ*mptG* allele; Km^r	(*14*)
§pCM410	P_{mxaF}-*flhA*-*fghA*; Km^r	This study
§pCM410.1145	pCM410 derivative isolated from CM1145; $fghA^{EVO}$ allele	This study
pCM433	*sacB*-based allelic exchange plasmid; Tc^r	(23)
pHC35	pCM433 with $pntAB^{WT}$ allele	This study
pHC36	pCM433 with $pntAB^{EVO}$ allele	This study
pHC37	pCM433 with $gshA^{WT}$ allele	This study
pHC38	pCM433 with $gshA^{EVO}$ allele	This study

*Strain designation included to clarify correspondence with condensed nomenclature for WT (*i.e.*, "0") and EVO ("1") alleles for the four loci in Fig. 2 (EM = CM702 = "0000"; EVO = CM1145 = "1111").
†Tc^r, tetracycline resistance.
‡Km^r, kanamycin resistance.
§GenBank accession numbers available: pCM410 (FJ389188) and pCM410.1145 (FJ389189)

Table S3. Parameters estimated from the fitness of single allele strains (mean fitness of all replicate experiments).

Allele	$pntAB^{EVO}$	$fghA^{EVO}$	GB^{EVO}	$gshA^{EVO}$
θ_i	0.993	0.485	0.362	0.323
λ_i	1.083	1.061	1.067	1.363

Supplemental References

21. D. H. Figurski, D. R. Helinski, *Proc Natl Acad Sci U S A* **76**, 1648 (Apr, 1979).
22. S. J. Van Dien, C. J. Marx, B. N. O'Brien, M. E. Lidstrom, *Appl Environ Microbiol* **69**, 7563 (Dec, 2003).
23. C. J. Marx, *BMC Research Notes* **1**, (26 February 2008, 2008).
2. J. W. Scott, M. E. Rasche, *J Bacteriol* **184**, 4442 (Aug, 2002).
25. C. J. Marx, M. E. Lidstrom, *BioTechniques* **33**, 1062 (Nov, 2002).
26. C. J. Marx, M. E. Lidstrom, *Microbiology* **147**, 2065 (Aug, 2001).
27. M. C. Lee, H. H. Chou, C. J. Marx, *Evolution* **63**, 2816 (Nov, 2009).
28. J. Ras *et al.*, *J Bacteriol* **177**, 247 (Jan, 1995).
29. N. Harms, J. Ras, W. N. Reijnders, R. J. van Spanning, A. H. Stouthamer, *J Bacteriol* **178**, 6296 (Nov, 1996).
30. M. M. Bradford, *Anal Biochem* **72**, 248 (May 7, 1976).
31. S. Wagner *et al.*, *Mol Cell Proteomics* **6**, 1527 (Sep, 2007).
32. T. Bouvier, M. Troussellier, A. Anzil, C. Courties, P. Servais, *Cytometry* **44**, 188 (Jul 1, 2001).
33. M. D. Abramoff, P. J. Magelhaes, S. J. Ram, *Biophotonics Int* **11**, 36 (2004).
34. S. Vuilleumier *et al.*, *PLoS One* **4**, e5584 (2009).
35. H. Dong, L. Nilsson, C. G. Kurland, *J Bacteriol* **177**, 1497 (Mar, 1995).
36. A. Novick, M. Weiner, *Proc Natl Acad Sci U S A* **43**, 553 (Jul 15, 1957).
37. I. Shachrai, A. Zaslaver, U. Alon, E. Dekel, *Mol Cell* **38**, 758 (Jun 11, 2010).
38. M. Scott, C. W. Gunderson, E. M. Mateescu, Z. Zhang, T. Hwa, *Science* **330**, 1099 (Nov 19, 2010).
39. R. A. Fisher, *The Genetical Theory of Natural Selection* (Clarendon, Oxford, 1930).
40. W. G. Hill, M. E. Goddard, P. M. Visscher, *PLoS Genet* **4**, e1000008 (Feb 29, 2008).
41. J. M. Stevens, T. Uchida, O. Daltrop, S. J. Ferguson, *Biochem Soc Trans* **33**, 792 (Aug, 2005).
42. M. Goenrich, S. Bartoschek, C. H. Hagemeier, C. Griesinger, J. A. Vorholt, *J Biol Chem* **277**, 3069 (Feb 1, 2002).